Role of the localized states in field emission of carbon nanotubes

Seungwu Han and Jisoon Ihm
Department of Physics and Center for Theoretical Physics, Seoul National University, Seoul 151-742, Korea
(Received 29 November 1999)

We have performed *ab initio* pseudopotential electronic structure calculations for various edge geometries of the (n,n) single-wall nanotube with or without applied fields. Among the systems studied, the one with a zigzag edge exposed by a slant cut is found to be the most favorable for emission due to the existence of unpaired dangling bond states around the Fermi level. The next most favorable geometry is the capped nanotube where π-bonding states localized at the cap and pointing in the tube axis direction occur at the Fermi level. A scaling rule for the induced field linear in the aspect ratio of the tube is also obtained.

The carbon nanotube (CNT) is an ideal material to make field emitters because of its unusually high aspect ratio as well as mechanical and chemical stability. Many experiments with single-wall[1,2] and multiwall[3–7] carbon nanotubes have demonstrated a relatively low threshold voltage of electron emission with little sample degradation. Recently, flat panel displays fabricated with the CNT's as emitters have been demonstrated.[8] Furthermore, advancements in fabrication technology make it possible to generate a self-aligned or a patterned CNT on a glass[9] or silicon substrate,[10] implying that commercial production of CNT-based field emission display may be possible in the near future.

In spite of the accumulating experimental data, realistic quantum mechanical calculations on the field emission of the CNT are still scarce. The simplistic view of the CNT as a jellium metallic emitter based on conventional Fowler-Nordheim theory could not explain the entire range of the *I-V* data[1,7] and a critical analysis of the electronic structure on a more fundamental level is required. In this study, we perform *ab initio* pseudopotential electronic structure calculations[11,12] with or without applied fields. We focus on the end geometries of the CNT where the electron emission actually occurs and try to find the optimized tip structure for field emission. The model systems are periodically repeated in a tetragonal supercell with the tube axis lying in the *z* direction. The plane-wave-based calculations with a cutoff energy of 35 Ry have been done mostly for a $\sim 20\times 20\times 30$ Å^3 unit supercell. To check the convergence of our results for larger systems, we have also used localized basis functions[13] in the *ab initio* pseudopotential calculations with the density grid corresponding to 60 Ry and have been able to enlarge the tube size up to four times.

We consider various end geometries of the CNT. The side views of the upper part of the (5,5) CNT's are shown in Fig. 1. The bottom (not shown) of the tube body is terminated with hydrogen atoms for computational convenience. We call (a)–(d) the H- (hydrogen-attached), FC- (flat-cut), CAP- (capped), and SC- (slant-cut) CNT's, respectively. The H-CNT represents a situation where the dangling bonds are chemically stabilized by ambient hydrogen. In the CAP-CNT model, the tube end is capped with a patch (hemisphere) of C_{60} having six pentagons. In the FC-CNT and SC-CNT, on the other hand, dangling bonds remain unsaturated. Relaxed geometries are obtained from computationally less demanding tight-binding calculations.[14]

In Fig. 2, the total density of states (TDOS) around the Fermi level is plotted with solid lines. All systems except the H-CNT have localized states near the nanotube edge. To investigate these localized states more closely, the local density of states (LDOS) around the end region is calculated and shown by dashed lines in Figs. 2(b) and 2(c). Energy levels of the localized states induced by the topological defects (pentagons) in the CAP-CNT are known to depend on the relative positions of the defects[15–17] and the pentagons are assumed to be separated from each other here as found in Ref. 16. The LDOS of the CAP-CNT is in reasonable agreement with previous results.[15–17] In Fig. 2(d), the LDOS of the SC-CNT at the two topmost atoms (the sharp edge) and that at the eight side atoms on the slant-cut cross section are shown in dotted and dashed lines, respectively. Descriptions of the different characters of these two will follow, and Fig. 2(e) will be explained later in the context of the applied field.

In Fig. 3(a), we show one of the localized states in the

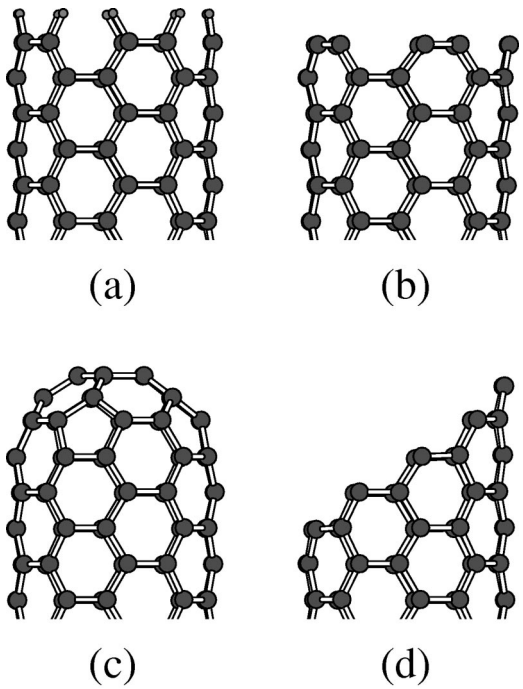

FIG. 1. Edge structures studied in this work. (a) H-CNT, (b) FC-CNT, (c) CAP-CNT, and (d) SC-CNT (see text for abbreviations).

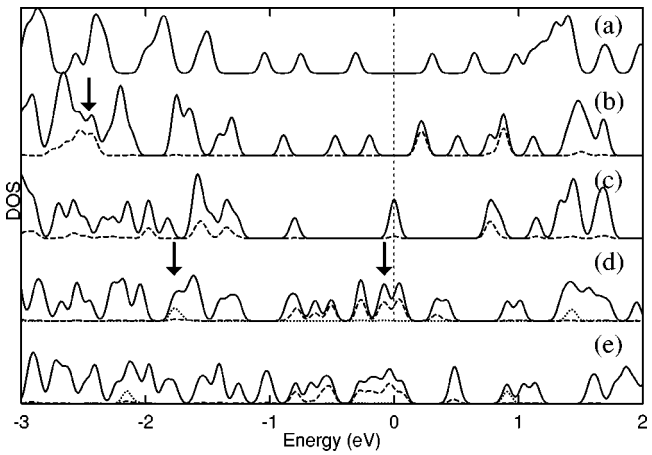

FIG. 2. TDOS (solid line) and LDOS (dashed or dotted lines) corresponding to each structure [(a)–(d)] in Fig. 1. The Fermi level is set to zero. The LDOS represents the states localized at the top of the nanotubes in Fig. 1. In (d), the dashed and dotted lines are differentiated as explained in the text. (e) is the DOS of the SC-CNT with the applied field of 0.4 V/Å , presented for comparison with (d).

FC-CNT whose energy level is indicated by an arrow in Fig. 2(b). Interestingly, two adjacent dangling bonds join at the backbond position of the original sp^2 configuration. The character of the *s* orbital is slightly lost in the sp^2 hybridization. Because of these additional bonds, the C-C bond length in the top layer is 1.27 Å compared with the ideal C-C distance in a perfect nanotube (1.41 Å), corresponding to a strong double bond. Two types of localized states are identified in the SC-CNT model. In Fig. 3(b), the topmost atoms on the armchairlike edge [states at -1.8 eV indicated by an arrow in Fig. 2(d)] show a similar backbonding as in the FC-CNT, while the individual dangling bonds on the side edge [indicated by an arrow at -0.1 eV in Fig. 2(d)] remain unpaired since they are far apart from each other along the zigzag edge. Since the interaction between them is weak, the energy splitting is small, resulting in a large LDOS at the Fermi level as indicated by the dashed line in Fig. 2(d). On the other hand, the energy splitting between the bonding and antibonding states is rather significant (~ 3 eV) for the states localized at the armchair edge, as shown in the two separate dotted curves.

A sawtooth-type potential is applied along the CNT axis to simulate a uniform external electric field in the supercell geometry. In the experimental situation, the applied field

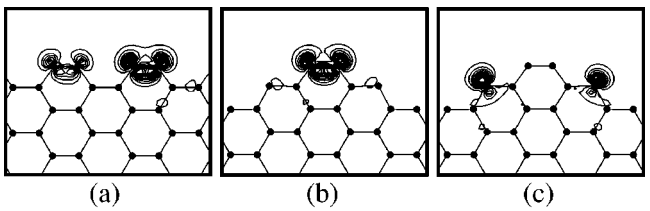

FIG. 3. Electron density of the localized states whose energy levels are indicated by arrows in Figs. 2(b) and 2(d). (a) is the localized state of the FC-CNT at -2.6 eV and (b) and (c) are the localized states of the SC-CNT at -1.8 eV and -0.1 eV, respectively. The electron density is evaluated on the nanotube surfaces and the contour interval is 0.08 $e/\text{Å}^3$.

TABLE I. Averaged local field within 3 Å outside the tip as a function of the tube length for a CAP-CNT. The applied field is varied so that its product with the tube length is fixed at 10 V.

Tube length (Å)	11.3	23.7	36.0	48.3	60.6	72.9
E_{loc} (V/Å)	2.00	1.29	1.08	0.90	0.87	0.87

strength is usually a few V/μm and the length of the CNT is a few μm, resulting in ~ 10 V difference in the applied potential between the tube ends. It has been well established that field emission typically occurs when the actual field at the tip is ~ 0.5 V/Å , corresponding to a field enhancement factor of ~ 1000 in the present experimental situation. Since the system size is severely limited in the *ab initio* calculation, it is a serious issue whether one can mimic the realistic situation and extract meaningful information on field emission through *ab initio* calculation for small-size tubes. After many different calculations, we find the following trends as summarized in Table I. We apply a uniform field across the supercell such that the potential difference across the tube (i.e., between the two tube ends) is fixed at 10 V for each case. For instance, for 23.7, 48.3, and 72.9 Å tubes, the applied field strengths are 0.42, 0.21, and 0.14 V/Å , respectively. The resulting total (applied + induced) field at (to be precise, just outside) the tip of the tube is listed in the table, showing saturation behavior of the total field when the tube length is beyond ~ 60 Å . We also find that the total field inside the tube is practically zero (less than a few percent of the applied field), indicating that the screening of the applied field inside the tube is very effective. Since the discontinuity in the electric field is equal to the surface charge density, the above behavior implies convergence (saturation) of the induced electronic charge at the tip for tube lengths $\gtrsim 60$ Å . (Even for a tube as short as 36 Å , the deviation from the converged value is within $\sim 25\%$.) This behavior is useful for extrapolating to the realistic long-tube–small-field case which is hardly accessible with *ab initio* methods. Another test we have made is to increase the applied field for a given tube geometry (35 Å long FC-CNT), and obtain the corresponding local field just outside the tip. A linear relation is found as long as the applied field is $\gtrsim 0.1$ V/Å . Table II shows such a relation and it can be fitted with $E_{tot} = 4.53 E_{appl} - 0.19$ (V/Å). The shift (-0.19) is due to the fact that the screening by localized states cannot occur until they begin to fill. Combining these two results and using independent calculations as well, we find that, for a given applied field, the field enhancement factor η at the edge scales linearly with the tube length l,

$$\eta \cong \alpha l. \tag{1}$$

For instance, α for a SC-CNT with diameter of 7 Å is approximately 0.17 (with l given in Å) as will be described

TABLE II. Averaged local field within 3 Å outside the tip as a function of the applied field for a 35 Å long FC-CNT. The data are well fitted with a straight line.

E_{appl} (V/Å)	0.17	0.23	0.5	0.83
E_{loc} (V/Å)	0.57	0.87	2.06	3.59

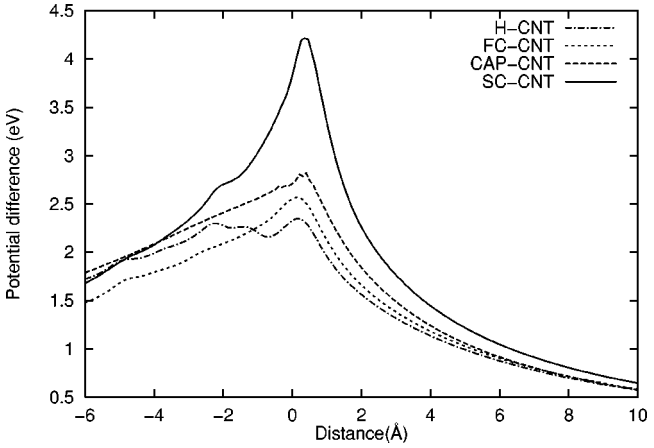

FIG. 4. Coulomb potential generated by the induced charge and plotted in the tube axis direction when an external field of 0.17 V/Å is applied for ~ 35 Å long tubes. The distance is measured from the edge of the tube.

below. Equation (1) is distinguished from the result for a conventional metallic prolate spheroid, $\eta \sim m^2/\ln(2m) - 1$ for large m, where m is the aspect ratio.

Now we examine the change in the electronic structure caused by the field in detail. In Fig. 2(e) shown above, the DOS for the SC-CNT under the applied field (~0.4 V/Å) is plotted as a representative case. Comparing it with Fig. 2(d) for the zero field case, we notice that the localized levels at the armchair edge (dotted curves) undergo a downward shift. The states localized on the zigzag chain sides of the edge are partially occupied for the zero field in Fig. 2(d) (dashed curves) and their occupation increases as the field is turned on. Such a situation is commonly observed in the field emission of metallic tips with atomic adsorbates.[18] Since these states are located at the Fermi level under the applied field, they are the first to be emitted across the barrier to the anode. The increase in occupation of the dangling bond states is approximately $0.1e$ per edge atom. The downward shift of the localized states by the field occurs in the FC-CNT and CAP-CNT as well. Shifts of the localized states are pinned as they begin to be occupied, hence these localized states stay at the Fermi level for a wide range of the field strength. The occupation of the localized states has the effect of repulsing the π electrons and suppresses the increase in amplitude of the π states at the edge. Actually, the sum of the accumulated charge does not vary too much from structure to structure.

The accumulated charge at the end of the CNT as described above enhances the local electric field, which is the driving force of field emission. For a quantitative analysis, we calculate the *change* in charge density under an applied field of 0.17 V/Å using an *ab initio* method with localized orbitals and plot the resulting Coulomb potential for an isolated tube along the tube axis in Fig. 4. The down slope on the left of the peak is essentially the negative of the applied field which screens out the applied field inside the tube. The down slope on the right of the peak, on the other hand, is the induced field that reduces the potential barrier when electrons are emitted across the vacuum barrier to the anode side. The difference between the H-CNT and other systems can be considered as contributions from the localized states inherent to the tip structures in Figs. 1(b)–1(d).

A striking feature in Fig. 4 is the prominent potential peak and the corresponding high field enhancement of the SC-CNT among the model systems. The average induced fields within 3 Å from the peak position to the right (vacuum region) are 0.53, 0.58, 0.65, and 1.03 V/Å for (a)–(d) geometries, respectively. The aforementioned extrapolations to a realistic 2 μm long tube lead to the field enhancement factors of 1700, 1900, 2100, and 3300, respectively, which compare favorably with the experimental values of 3600 (Ref. 2) or 1300.[4] A greater enhancement factor for the SC-CNT than the CAP-CNT is consistent with experiment[5] considering that the multiwall open CNT used in experiment should have some unsaturated dangling bonds like the SC-CNT studied here. One might expect that the highest induced field in the SC-CNT should originate from its sharpest armchair edge (hence the highest field enhancement factor according to classical electrostatics) among the structures studied. However, when we probe the induced electric field very closely all over the space, we find that the region around the zigzag side edge has a field at least as large as that of the topmost atoms. To identify the origin of the high field unambiguously, we have performed the same calculation for a flat-cut (12,0) zigzag-type nanotube. We find a sharp Coulomb potential peak identical to that in the SC-CNT. We conclude that the unpaired dangling bond states at the Fermi level under an applied field, which exist in both the SC-(n,n)-CNT and the FC-$(3n,0)$-CNT, are mainly responsible for the highest potential peak, i.e., the largest induced field toward the anode side. Therefore, the most favorable tip geometry for field emission in our study is the open tube with zigzag-type edge where unsaturated dangling bond states can exist. We also emphasize that the lobes of these dangling bond wave functions are directed toward the anode side and their overlap integral with the tail of the free-electron-like state from the anode side of the barrier is relatively large (meaning a large emission probability), while the π-electron states on the tube body lie perpendicular to the emission direction and the corresponding overlap integral is much smaller.

It is interesting that the CAP-CNT has the next highest peak in Fig. 4, higher than that of the FC-CNT. The occupation of the π states in the hemispherical region of the CAP-CNT easily increases as the external field is turned on and contributes to the induced field efficiently because the states are at the Fermi level.[17] Since the π electron at the top of the hemisphere points to the anode side, the overlap integral mentioned above is reasonably large in this case. We also note that, although the H-CNT has a relatively small induced Coulomb potential, its magnitude is still appreciable in Fig. 4. The accumulated charge here is the usual metallic π states. Our results show that both the localized states and the metallic π states can contribute to the field enhancement. We have also calculated the effects of the image potential and the periodic array of emitters self-consistently, but the details will be described elsewhere.

In summary, we have studied the electronic structure of various edge shapes of a single-wall nanotube with or without external fields. A linear scaling behavior of the field enhancement factor as a function of the tube length has been

obtained. Open tubes with dangling bonds at the zigzag-type edge are predicted to be the most favorable for field emission among the structures considered here. Capped nanotubes with π-bonding states localized at the cap region are the next most favorable structure. The question arises whether open tubes remain stable. It is likely that hydrogen atoms or other ambient atoms and molecules cap the reactive dangling bonds of the open nanotubes. Since the energy barrier from an open tube to a closed one increases with the tube radius, carbon nanotubes with a large radius used for real field emission purposes may stay open with these stabilizing foreign atoms or molecules saturating the dangling bonds. The attached atoms or molecules may be desorbed by an extremely strong local field during the actual emission process and the dangling bonds may be exposed, to contribute greatly to electron emission. Unlike the case of foreign atoms or molecules, the strong sp^2 bond of the tube body is not dissociated under the typical field ($\lesssim 1$ V/Å) in experiment. For multiwall CNT cases, the saturated (threefold) coordination of all edge atoms by bridging carbon atoms cannot occur in general because of the the incommensurability between neighboring coaxial tubes, and there should remain some unsaturated dangling bonds during the emission process contributing to the field emission.[19] Existing experimental data do not yet give information on the dependence of the emission efficiency on the detailed tip structure. Our study proposes a high-efficiency edge structure which can significantly improve the field emission performance. We also note that, for practical display application, it is enough for only a small fraction of nanotubes to actually emit electrons because of the huge redundancy in the total number of nanotube emitters.

This work was supported by the SRC Program of the KOSEF, the BSRI Program, and the BK21 Project of the KRF.

[1] Y. Saito *et al.*, Jpn. J. Appl. Phys., Part 2 **36**, L1340 (1997).
[2] J.-M. Bonard, J.-P. Salvetat, T. Stockli, and W. A. de Heer, Appl. Phys. Lett. **73**, 918 (1998).
[3] A. G. Rinzler *et al.*, Science **269**, 1550 (1995).
[4] W. A. de Heer, A. Chatelain, and D. Ugarte, Science **270**, 1179 (1995).
[5] Y. Saito *et al.*, Appl. Phys. A: Mater. Sci. Process. **67**, 95 (1998).
[6] Q. H. Wang, T. D. Corrigan, J. Y. Dai, and R. P. H. Chang, Appl. Phys. Lett. **70**, 3308 (1997).
[7] P. G. Collins and A. Zettl, Appl. Phys. Lett. **69**, 1969 (1996); Phys. Rev. B **55**, 9391 (1997).
[8] Q. H. Wang, A. A. Setlur, J. M. Lauerhaas, J. Y. Dai, E. W. Seelig, and R. P. H. Chang, Appl. Phys. Lett. **72**, 2912 (1998); Y. Saito, S. Uemura, and K. Hamaguchi, Jpn. J. Appl. Phys., Part 2 **37**, L346 (1998); W. B. Choi *et al.*, Appl. Phys. Lett. **75**, 3129 (1999).
[9] Z. F. Ren *et al.*, Science **282**, 1105 (1998).
[10] S. Fan *et al.*, Science **283**, 512 (1999).
[11] J. Ihm, A. Zunger, and M. L. Cohen, J. Phys. C **12**, 4409 (1979).
[12] N. Troullier and J. L. Martins, Phys. Rev. B **43**, 1993 (1991).
[13] O. F. Sankey and D. J. Niklewski, Phys. Rev. B **40**, 3979 (1989).
[14] C. H. Xu, C. Z. Wang, C. T. Chan, and K. M. Ho, J. Phys.: Condens. Matter **4**, 6047 (1992).
[15] D. L. Carroll *et al.*, Phys. Rev. Lett. **78**, 2811 (1997).
[16] P. Kim, T. W. Odom, J.-L. Huang, and C. M. Lieber, Phys. Rev. Lett. **82**, 1225 (1999); R. Tamura and M. Tsukada, Phys. Rev. B **52**, 6015 (1995).
[17] A. De Vita, J.-Ch. Charlier, X. Blase, and R. Car, Appl. Phys. A: Mater. Sci. Process. **68**, 283 (1999).
[18] V. T. Binh, S. T. Purcell, N. Garcia, and J. Doglioni, Phys. Rev. Lett. **69**, 2527 (1992); M. L. Yu, N. D. Lang, B. W. Hussey, T. H. P. Chang, and W. A. Mackie, *ibid.* **77**, 1636 (1996).
[19] J. Charlier, A. De Vita, X. Blase, and R. Car, Science **275**, 646 (1997).